Available online at www.sciencedirect.com

SCIENCE DIRECT®

Journal of Molecular Catalysis A: Chemical 198 (2003) 139–149

JOURNAL OF MOLECULAR CATALYSIS A: CHEMICAL

www.elsevier.com/locate/molcata

MCM-41 supported Mo/Zr mixed oxides as catalysts in liquid phase condensation of 2-methylfuran with acetone

Tao Li [a], Soofin Cheng [a,*], Jyh-Fu Lee [b], Ling-Yun Jang [b]

[a] *Department of Chemistry, National Taiwan University, Taipei 106, Taiwan*
[b] *Research Division, Synchrotron Radiation Research Center, Hsinchu 300, Taiwan*

Received 24 June 2002; received in revised form 25 September 2002; accepted 4 November 2002

Abstract

Molybdenum and zirconium mixed oxides were supported on siliceous MCM-41 mesoporous material. The resultant materials were characterized with various techniques such as X-ray diffraction (XRD), nitrogen adsorption, Transmission electron microscopy (TEM), XANES, NH_3-TPD, and Diffuse reflectance infrared Fourier transform spectra (DRIFTS) of pyridine. It was found that the well-ordered channeling pores of MCM-41 were retained with a maximum loading of 9 wt.% MoO_3 and 13 wt.% ZrO_2. The $ZrMo_2O_8$ crystallites appeared with an even higher loading. The materials had surface areas greater than 500 m^2/g and a relatively narrow pore size distribution. MoO_3 and ZrO_2 were well dispersed inside the pores of MCM-41. The Mo(VI) was found in octahedral coordination when no $ZrMo_2O_8$ crystallites were detected. The MoO_3/ZrO_2/MCM-41 samples contained only Lewis acid sites. Although NH_3-TPD experiments indicated that its acid strength was weaker than that of Y-zeolite, the MoO_3/ZrO_2/MCM-41 materials were excellent catalysts for liquid phase condensation of 2-methylfuran (MF) with acetone to form 2,2-bis(5-methylfuryl)propane (BMP).

Keywords: Molybdena; Zirconia; Mixed oxide; Catalyst; Acid; MCM-41; 2-Methylfuran; Acetone; Liquid phase condensation

1. Introduction

Due to the hazardous properties of liquid acids such as HF and H_2SO_4 commonly employed in the current petrochemical industry, a great effort has been focused on the development of more environmental friendly strong solid acids [1]. Sulfated metal oxides, especially sulfated zirconia, have attracted great attention in this decade because they demonstrate high catalytic activities in skeletal isomerization of alkanes at relatively low temperatures [2–4]. However, the gradual loss of sulfur during the reaction processes is its drawback. Subsequent to the discovery of strong acidity on the sulfated zirconia, Hino and Arata found that zirconia loaded with tungsten oxide [5] or molybdenum oxide [6] also showed high catalytic activities for the skeletal isomerization of alkanes and benzoylation of toluene, both of which need strong acidic catalysts. These materials, if prepared properly, could achieve surface areas of around 100–200 m^2/g. However, the non-uniform pore size and relatively small surface area may limit their applications in catalytic reactions involving bulky molecules, such as those encountered in synthesis of pharmaceuticals and fine chemicals.

MCM-41 is the most well studied member of the M41S meso-structured silica family discovered by the researchers at Mobil [7]. It has a uniformed

* Corresponding author. Fax: +886-2-23636359.
E-mail address: chem1031@ccms.ntu.edu.tw (S. Cheng).

1381-1169/03/$ – see front matter
doi:10.1016/S1381-1169(02)00730-6

hexagonal array of mesopores and very high surface area (typically around 1000 m^2/g). This material has been shown to be an excellent support for preparing supported catalysts with superior activities and selectivities, compared to those supported on amorphous silica, alumina, or zeolites in reactions such as hydrocracking of vacuum gas oil [8], hydrogenation of aromatics [9], and liquid phase metathesis [10]. That is because the mesoporous materials facilitate the diffusion of bulky organic molecules in and out of the porous structures [11]. However, the siliceous mesoporous material itself has no acidity and low catalytic activities. Over the past 3 years, strong acid sites were introduced onto the mesoporous materials by supporting sulfated zirconia on MCM-41 [12–16]. The resultant material was found to be a strong acid catalyst and very active in *n*-butane isomerization [12,13,15,16], MTBE synthesis and *n*-pentane isomerization [14]. Although zirconia loaded with tungsten oxide [5] or molybdenum oxide [6] were also reported to be strong acid catalysts, up to now, no reports concerning mesoporous materials supported on these mixed oxides were found. The aim of this study is to introduce acid function onto the mesoporous MCM-41 material by supporting Mo/Zr mixed oxide on it and to examine the catalytic activities of the resultant materials. The catalytic reaction under investigation is the liquid phase condensation of 2-methylfuran (MF) with acetone to form 2,2-bis(5-methylfuryl)propane (BMP). Furan is a well-known representative of a series of five-member unsaturated 'heteroaromatic' compounds. In this family, bisfurylalkanes are the relevant intermediates for macromolecular chemistry [17]. The derived materials have a useful range of applications, mostly for foundry cores and molds, corrosion-resistant materials, and precursors to graphitic composites and adhesives [18]. It is produced by the condensation of 2-methylfuran with acetone catalyzed by a strong acid, either Brönsted or Lewis acids [19,20]. Because the furan rings are highly reactive towards electrophilic aromatic substitution [21], large amounts of oligomeric products are generally formed during the reactions of furan heterocycles over zeolite catalysts such as H-β and H-US-Y [20]. Moreover, the strong adsorption of BMP or other reaction intermediates in the zeolite pores usually leads to extensive polymerization. As a result, the zeolite pores are blocked and the catalyst deactivates readily. Therefore, it is necessary to search for other strong acidic materials with relatively large pores catalyzing this reaction. Van Rhijn et al. [22] used sulfonic acid functionalized MCM-41 materials as catalysts for this reaction. The highest BMP yield of 82% was obtained. These results will be compared with those over Mo/Zr mixed oxide supported on MCM-41.

2. Experimental

2.1. Catalyst preparation

Pure siliceous MCM-41 was synthesized according to the method reported by Das et al. [23]. The molar ratio of the synthesis gel composition is SiO_2:0.48$CTMA^+$:0.33TPA^+:0.39Na_2O:0.29H_2SO_4:110H_2O. A sample of Al-MCM-41 was also prepared by using sodium aluminate (Nakarai) as the Al source and the Si/Al molar ratio in the synthesis gel was 33.

The MoO_3/ZrO_2/MCM-41 samples were prepared by depositing zirconium hydroxide on MCM-41, followed by impregnation to introduce molybdena. As-synthesized MCM-41 powders were dispersed in an aqueous solution of zirconyl chloride octahydrate (Riedel-deHaën, 99.5%) under vigorous stirring. Then aqueous ammonia was added until the pH reached ca. 10 to precipitate zirconium hydroxide. The obtained solids were washed until the filtrate was free of Cl^- ions. After drying in air overnight at 100 °C, the solid was impregnated with desired amount of aqueous solution of ammonium heptamolybdate (Riedel-deHaën, 99%). The dried samples were calcined in air at 560 °C for 6 h (heating rate at 1 °C/min) to remove the organic surfactant. The resultant samples were further calcined at higher temperatures for 3 h to examine the effect of calcination temperature. The same preparation procedure was used for preparing the $MoO_3/ZrO_2/SiO_2$ sample, where SiO_2 is a silica gel purchased from Acros. MoO_3/ZrO_2 without support was also prepared by impregnation of zirconium hydroxide, which was obtained by precipitation of zirconyl chloride octahydrate with aqueous ammonia, with ammonium heptamolybdate. After impregnation and drying, the sample was calcined at 750 °C for 3 h in air. Another sample MoO_3/ZrO_2 + MCM-41 was prepared by physically mixing the MoO_3/ZrO_2 sample with calcined MCM-41.

2.2. Catalyst characterization

Powder X-ray diffraction (XRD) patterns were recorded with a Scintag X1 diffractometer using Cu Kα radiation. Nitrogen adsorption–desorption isotherms were obtained at liquid nitrogen temperature with a Micromeritics ASAP 2000 apparatus. Transmission electron microscopy (TEM) was performed on a Hitachi H-7100 instrument operated at 100 keV. The elemental contents in bulk were determined by inductively coupled plasma atomic emission spectroscopy (ICP-AES, Jarrell-Ash, ICAP9000) on the HF and H_2O_2 dissolved samples. The X-ray adsorption spectra were taken with synchrotron radiation at the Synchrotron Radiation Research Center, Hsinchu, Taiwan. The storage ring was operated at 1.5 GeV with about 120–200 mA ring current. Data were collected using total electron yield and fluorescence detection.

The temperature-programmed desorption of ammonia (NH_3-TPD) was carried out on a Micromeritics AutoChem 2910 instrument. 50 mg of dried sample was pre-treated at 500 °C under ultra-high pure helium (50 ml/min) for 1 h and then cooled to 120 °C. After introducing anhydrous NH_3 at 120 °C for 0.5 h, the sample was flushed with helium for 1 h. TPD profile of ammonia was obtained from 120 to 800 °C at a heating rate of 10 °C/min. The desorption process was monitored by a quadruple mass spectrometer (Thermo ONIX, ProLab) connected on line through a heated capillary interface. The mass number of 16 was followed to obtain TPD profiles of NH_3 because the mass intensity is relatively strong and the interference from H_2O is negligible. A HY-zeolite sample (Si/Al = 2.7) provided from Asia reference catalyst (no. 25) and another of Si/Al = 24 from Advchem Laboratories Inc. were used as references.

Diffuse reflectance infrared Fourier transform (DRIFT) spectra of the samples adsorbing pyridine were recorded using a BOMEM MB155 FT-IR/Raman spectrometer. The equipment was furnished with an in situ sample cell (Harrick). The sample was pre-heated at 300 °C for 3 h under 10^{-6} mbar vacuum before pyridine vapor was introduced at room temperature, followed by evacuation for 30 min. Spectra were acquired from room temperature to 500 °C under vacuum.

2.3. Catalytic study

Catalytic activities of the samples were tested in the acid-catalyzed condensation of 2-methylfuran (MF) with acetone. In a typical case, 1.8 g MF and 3.2 g acetone were mixed in a three-necked glass flask with reflux set-up. After 0.18 g solid catalyst was added, the reaction mixture was heated at 50 °C with stirring for 24 h. Then the solid was separated by filtration. The liquid to which was added known amount of toluene as an internal standard, was analyzed by a gas chromatograph equipped with an Rtx-5 column and an FID detector. The BMP selectivity was calculated based on the conversion of MF instead of acetone.

3. Results and discussion

3.1. Characterization of catalysts

As-synthesized MCM-41 was used as the precursor for the preparation of supported catalysts. In contrast to the calcined samples, the as-synthesized MCM-41 with the surfactant templates still in the pores can tolerate the media encountered in the catalyst preparation procedure. Fig. 1 shows the XRD patterns of the MCM-41 samples before and after the introduction of zirconia and molybdena. All the samples preserve the ordered hexagonal structure of MCM-41, although the intensity of the diffraction peaks of MCM-41 decreases slightly after precipitation of zirconium hydroxide and impregnation with MoO_3. The relatively lower diffraction peak intensity is attributed to the decrease in diffraction contrast of the lattice when the pores are filled with either the organic template or the oxides. In addition, the unit cells shrank slightly after the samples were calcined. The XRD patterns of 10% MoO_3/7% ZrO_2/MCM-41 samples calcined at different temperatures were also compared (not shown). Although a slight decrease in the diffraction peak intensity can be seen with the increase of calcination temperature, all the samples retain the ordered structure of MCM-41 after calcination at 560–800 °C.

Fig. 2 shows the XRD patterns of MoO_3/ZrO_2/MCM-41 samples with similar MoO_3 loadings but different ZrO_2 contents. For MCM-41 loaded with molybdena only, the ordered structure of MCM-41 collapsed completely after calcination at 750 °C.

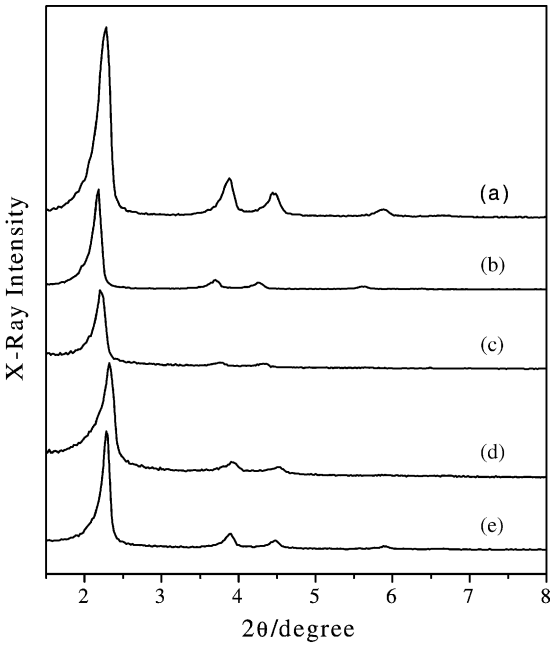

Fig. 1. XRD patterns of (a) MCM-41 (calcined at 750 °C); (b) as-synthesized MCM-41; (c) 9% MoO_3/13% ZrO_2/MCM-41 (uncalcined); (d) 9% MoO_3/13% ZrO_2/MCM-41 (calcined at 750 °C) and (e) 14% ZrO_2/MCM-41 (calcined at 750 °C).

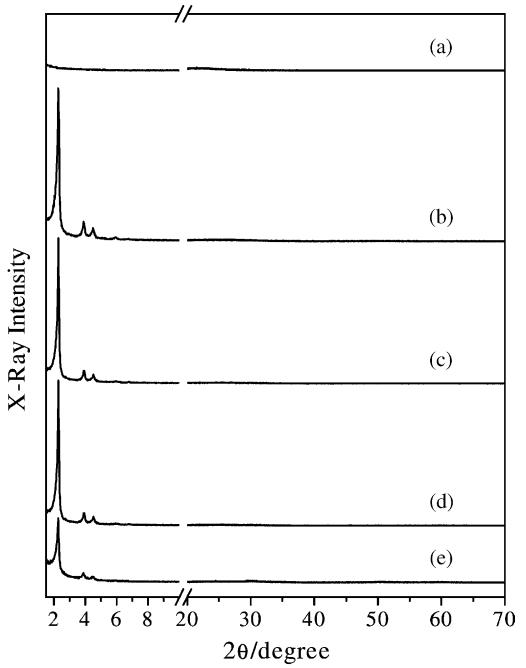

Fig. 2. XRD patterns of mixed oxides supported on MCM-41 after calcination at 750 °C for 3 h. (a) 8% MoO_3; (b) 9% MoO_3/4% ZrO_2; (c) 10% MoO_3/7% ZrO_2; (d) 9% MoO_3/13% ZrO_2 and (e) 10% MoO_3/22% ZrO_2.

Other researchers have also observed similar results. Wong et al. [24] reported that MCM-41 impregnated with 6 wt.% MoO_3 suffered a drastic destruction of MCM-41. Cho et al. [25] obtained amorphous structure for Mo-MCM-41 with Mo loadings up to ca. 10%. It is of great interest to notice that the ordered structure of MCM-41 was well preserved when zirconia was concomitantly introduced with molybdena. Four distinct diffraction peaks corresponding to 1 0 0, 1 1 0, 2 0 0, 2 1 0 planes of MCM-41 are visible for 8–10% MoO_3/ZrO_2/MCM-41 with ZrO_2 content in the range of 4–22 wt.%. These results imply that the MoO_x species on MoO_3/MCM-41 sample probably interact with the framework of MCM-41 strongly and destroy the structure. However, if MCM-41 is coated with $Zr(OH)_4$ first, MoO_x species then interact with ZrO_2 instead of the silica framework of MCM-41 so that the ordered structure of MCM-41 is retained. Moreover, no diffraction peaks due to MoO_3 or ZrO_2 crystallites were observed on all these samples. Therefore, MoO_3 and ZrO_2 should be well dispersed on the surface of MCM-41. The TEM photographs (not shown) also confirmed that the hexagonal meso-structure of MCM-41 was still retained and MoO_3/ZrO_2 crystals were mainly in the channels of MCM-41.

Fig. 3 shows the XRD patterns of MoO_3/ZrO_2/MCM-41 with similar ZrO_2 contents but different MoO_3 loadings. It can be seen that the patterns of samples with MoO_3 loadings varying in 2–9 wt.% are similar to that of MCM-41 loaded with 14% ZrO_2 only. Within this range of MoO_3 loading, the MoO_3 seems to interact with ZrO_2 and has little effect on the crystal structure of MCM-41. When the MoO_3 loading is raised to 14 wt.%, the intensity of the diffraction peaks of MCM-41 decreases drastically. Even further increase in the MoO_3 loading to 17 wt.%, caused the ordered structure of MCM-41 to collapse completely. In the mean time, the diffraction peaks corresponding to $ZrMo_2O_8$ phase [26] appeared. Based on the XRD results, the maximum loadings of MoO_3 and ZrO_2 on MCM-41 to retain the crystal structure of MCM-41 are 14 and 22 wt.%, respectively.

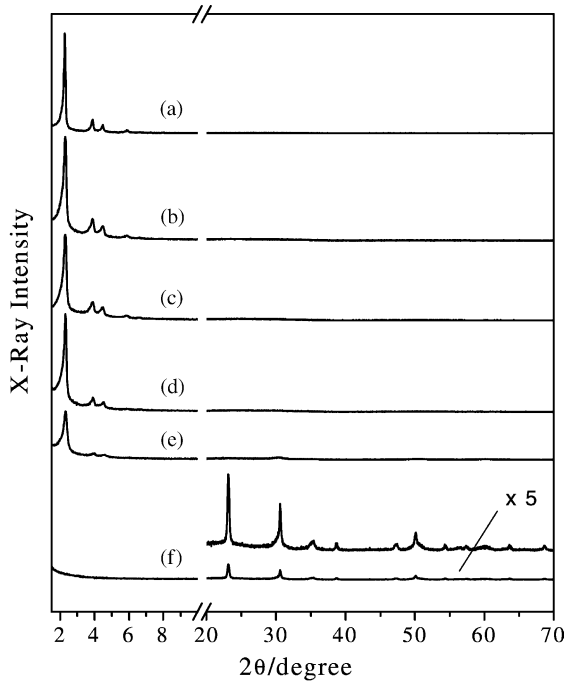

Fig. 3. XRD patterns of MoO_3/14% ZrO_2/MCM-41 with different MoO_3 loadings after calcination at 750 °C for 3 h (a) 0%; (b) 2%; (c) 4%; (d) 9%; (e) 14% and (f) 17%.

Iglesia and co-workers [27–29] reported that when the Mo surface density was higher than 5 Mo/nm^2 and the calcination temperature was above 600 °C, $ZrMo_2O_8$ was the predominant structure on MoO_x/ZrO_2 samples due to the strong interactions between MoO_x and ZrO_2. Our MoO_3/ZrO_2/MCM-41 samples calcined at 750 °C with MoO_3 and ZrO_2 loadings lower than 14 and 22%, respectively, do not show any diffraction peaks corresponding to $ZrMo_2O_8$. In these cases, the ordered structure of MCM-41 is still retained. Although MoO_3 and ZrO_2 have strong interactions, the well-dispersed ZrO_2 on the surface of MCM-41 has a high surface area. As a result, the Mo surface density was lower than that for forming $ZrMo_2O_8$ structure. Above these loadings, the mesoporous structure of MCM-41 would collapses. Then, MoO_3 and ZrO_2 would have the opportunity to sinter together and form the $ZrMo_2O_8$ phase.

The physical properties measured from nitrogen adsorption–desorption isotherms of the MoO_3/ZrO_2/MCM-41 catalysts are listed in Table 1. The calcined parent MCM-41 sample has a BET surface area of 1085 m^2/g and pore volume of 1.0 cm^3/g. It also has a very narrow pore size distribution centered at 27 Å. After molybdena and zirconia were supported on MCM-41, the surface area, pore volume and mesopore diameter decrease with the metal oxide loading. These results imply that the supported oxides should be dispersed onto the internal surfaces of the mesopores of MCM-41. BET analyses show that the supported catalysts have much larger surface areas (>500 m^2/g) than the unsupported MoO_3/ZrO_2 (<100 m^2/g). Table 1 also shows that the surface area, pore volume and mesopore diameter decrease with the increase in calcination temperature. These results are in consistence with those observed from XRD studies.

Synchrotron radiation based on X-ray absorption spectra at Mo L_3-edge were taken because the data provided information on the local coordination symmetry (especially tetrahedral versus octahedral) of Mo [30–35]. The L_3-edge spectrum of Mo(VI) is characterized by two absorption peaks, which are assigned to the electron transition from an initial state of p-level to the excited states of predominantly d-character. For Mo in the tetrahedral field, the splitting of the d-orbitals (e and t_2) should be smaller than that in octahedral field (t_{2g} and e_g). Moreover, the number of orbitals is also reflected in the relative intensity of the two transitions. Mo in tetrahedral environment has two peaks in L_3-edge spectra with an approximately 2:3 (e below t_2) ratio in the peak intensity while that in octahedral coordination has a 3:2 (t_{2g} below e_g) ratio. Fig. 4 illustrates the Mo L_3-edge spectra of MoO_3/ZrO_2/MCM-41 samples with different MoO_3 loadings, along with that of α-MoO_3 (octahedral Mo^{6+}), Na_2MoO_4 (tetrahedral Mo^{6+}) and $ZrMo_2O_8$ (tetrahedral Mo^{6+}). It is readily seen that all the MoO_3/ZrO_2/MCM-41 samples with MoO_3 loading lower than 14 wt.% have the L_3-edge spectra in agreement with Mo in octahedral coordination. However, 17% MoO_3/13% ZrO_2/MCM-41 sample has tetrahedral Mo^{6+}. From the XRD results, we know that $ZrMo_2O_8$ is formed in this sample.

The temperature-programmed desorption of ammonia (NH_3-TPD) was performed to determine the amount and the strength of acid sites on the catalysts. Fig. 5 compares the NH_3-TPD profile of MoO_3/ZrO_2 supported on MCM-41 with those of siliceous MCM-41, Al-MCM-41 (Si/Al = 31 analyzed by ICP-AES), MoO_3/ZrO_2 mechanically mixed with

Table 1
Physical properties of the Mo/Zr mixed oxide supported on MCM-41 in comparison to those of Mo/Zr oxide supported on silica, the pristine MCM-41 and Mo/Zr mixed oxide

Catalyst	Calcined temperature (°C)	BET surafce area (m^2/g)	BJH pore volume[a] (cm^3/g)	BJH pore diameter[a] (Å)
20% MoO_3/ZrO_2	750	77.9	–	–
4M13Z/SiO_2	750	181	–	–
MCM-41	560	1085	1.0	26.8
Al-MCM-41	560	1012	0.97	25.9
8M0Z/M41[b]	750	21.6	–	–
9M4Z/M41	750	758	0.61	24.5
10M7Z/M41	750	708	0.53	24.8
9M13Z/M41	750	624	0.59	24.8
10M22Z/M41	750	503	0.53	24.2
0M14Z/M41	750	846	0.80	26.6
2M14Z/M41	750	718	0.70	25.5
4M13Z/M41	750	694	0.67	25.3
14M13Z/M41	750	463	0.43	23.8
17M13Z/M41	750	58.4	–	–
10M7Z/M41	560	921	0.73	25.9
	650	756	0.61	25.9
	700	743	0.59	25.5
	750	708	0.53	24.8
	800	666	0.47	22.5
HY (Si/Al = 2.7)	–	692	–	–
HY (Si/Al = 24)	–	710	–	–

[a] Data from N_2 desorption isotherm.
[b] The MCM-41 supported catalysts were denoted as *x*M*y*Z/M41, where *x* and *y* are the wt.% loading; M and Z represent MoO_3 and ZrO_2, respectively, and M41 is MCM-41.

MCM-41, and MoO_3/ZrO_2 supported on silica gel. The MoO_3 and ZrO_2 contents in the three supported samples were similar, 4% MoO_3 and 13–17% ZrO_2. Siliceous MCM-41 shows no desorption peak (profile a), indicating that it has no acidity. The MoO_3/ZrO_2 mechanically mixed with MCM-41 shows a very weak desorption peak maximized around 230 °C (profile b), while that supported on MCM-41 has a strong desorption peak with the maximum at 203 °C (profile c). The MoO_3/ZrO_2 supported on silica gel (profile d) also exhibits a strong desorption peak at ca. 218 °C, but the peak intensity is weaker than that of MCM-41. Al-MCM-41 has a broad desorption peak centered at ca. 260 °C (profile b), and the peak intensity is weaker than that of supported MoO_3/ZrO_2.

The TPD profiles of HY-zeolites with Si/Al atomic ratio of 24 and 2.7 are also shown in Fig. 5 as references. The one with a high Al content (Si/Al = 2.7) has two huge desorption peaks at ca. 200 and 350 °C, corresponding to sites of weak and strong acidities, respectively. It implies that this sample has huge amounts of acid sites, and the amount of weak acid sites is greater than that of the strong ones. On the other hand, the HY-zeolite with low Al content (Si/Al = 24) has more sites of strong acidity, although its acid amount is relatively low. In comparison, the supported MoO_3/ZrO_2 samples and Al-MCM-41 have most of their acid sites in the weak acidity region. The results also demonstrate that MoO_3/ZrO_2 supported on either MCM-41 or silica gel contains much more acid sites than the unsupported sample or the physical mixture. These results accompanying with the BET results in Table 1 suggest that supporting MoO_3/ZrO_2 on MCM-41 can form mixed oxide of high dispersion and generate a large amount of acid sites with relatively weak acid strength. Moreover, the acid strength is close to that of Al-MCM-41 and silica supported sample.

Fig. 6 compares the NH_3-TPD profiles of MCM-41 supported MoO_3/ZrO_2 with nearly the same ZrO_2 content but different MoO_3 loadings. For the 14% ZrO_2/MCM-41 sample without MoO_3, only a small

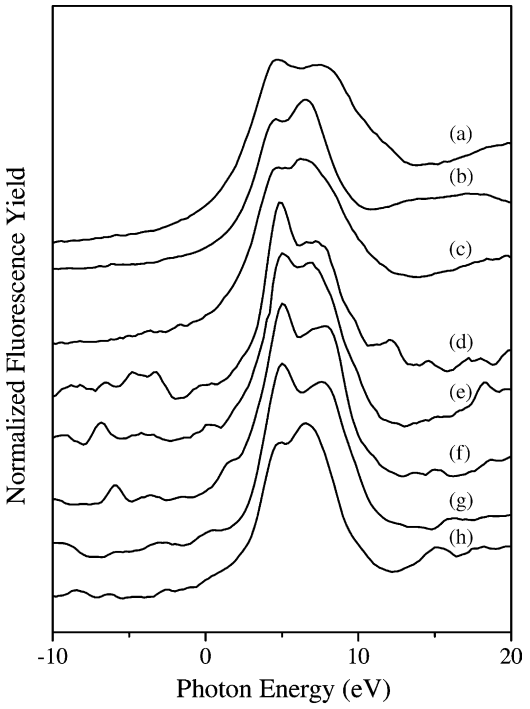

Fig. 4. XANES of Mo-L_3-edge of (a) α-MoO_3; (b) Na_2MoO_4; (c) $ZrMo_2O_8$, and MoO_3/14% ZrO_2/MCM-41 with different MoO_3 loadings after calcination at 750 °C for 3 h (d) 2%; (e) 4%; (f) 9%; (g) 14% and (h) 17%.

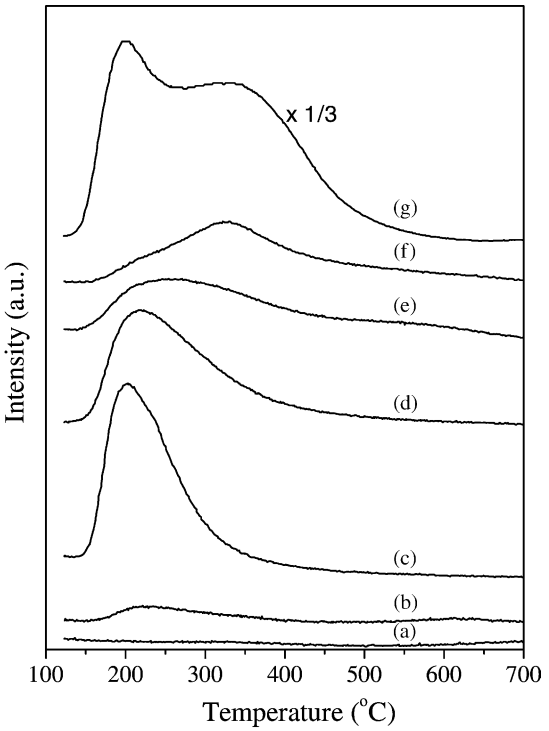

Fig. 5. NH_3-TPD profiles of (a) Si-MCM-41; (b) 4% MoO_3/17% ZrO_2+MCM-41 (mechanically mixed); (c) 4% MoO_3/13% ZrO_2/MCM-41; (d) 4% MoO_3/13% ZrO_2/SiO_2; (e) Al-MCM-41 (Si/Al = 31); (f) HY (Si/Al = 24) and (g) HY (Si/Al = 2.7).

desorption peak can be seen (profile a). This suggests that supporting ZrO_2 onto MCM-41 can only generate a small amount of weak acid sites. When both MoO_3 and ZrO_2 were supported on MCM-41, the amount of acid sites increased drastically, while the acid strength does not change significantly. Especially when the MoO_3 loading is increased from 4 to 9%, the TPD profiles show an additional desorption shoulder appearing at 244 °C other than the main peak at 206 °C. It implies that both the amount of acid sites and the acid strength increase with the MoO_3 loading. However, when the MoO_3 loading is increased further to 17%, only one desorption peak at 205 °C is seen, and the peak area is lower than that containing 4% MoO_3. As described above, the 17% MoO_3 sample loses the mesoporous structure of MCM-41 and the predominant species is found to be $ZrMo_2O_8$. Furthermore, this sample has a very low BET surface area. These results imply that $ZrMo_2O_8$ probably has little contribution to the acidity.

In order to examine the effect of surface adsorbed water on acidity, the 4% MoO_3/13% ZrO_2/MCM-41 sample was pre-treated with water vapor at 50 °C for 1 h, followed by NH_3-TPD experiment from 50 to 700 °C. Fig. 6(e) shows that the acidity of the sample is basically unaffected by adsorbing water on the surface. The new huge peak that appeared at ca. 100 °C is attributed to the physically adsorbed ammonia.

The DRIFT spectra of pyridine adsorbed on MoO_3/ZrO_2/MCM-41 were taken to distinguish the Brönsted and Lewis acid nature of the acid sites. Fig. 7 shows the DRIFT spectra of 9% MoO_3/13% ZrO_2/MCM-41 after adsorption of pyridine and desorption at various temperatures. It can be seen that only Lewis acid sites, showing the bands at 1450, 1487 and 1609 cm^{-1}, are present on the sample. That is similar to the acid character observed on molybdena loaded zirconia [6]. Two peaks corresponding to H-bonded pyridine appearing at 1446 and 1597 cm^{-1}

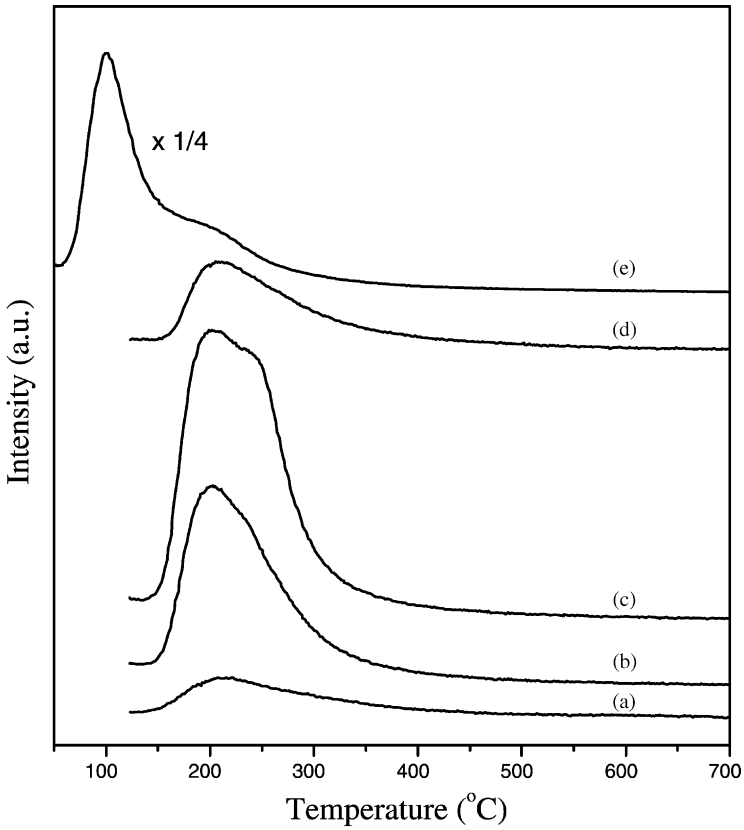

Fig. 6. NH_3-TPD profiles of (a) 14% ZrO_2/MCM-41; (b) 4% MoO_3/13% ZrO_2/MCM-41; (c) 9% MoO_3/13% ZrO_2/MCM-41; (d) 17% MoO_3/13% ZrO_2/MCM-41 calcined at 750 °C for 3 h and (e) sample (b) after exposing to moisture.

disappear after heating to 200 °C. No Brönsted acid sites (characteristic at ca. 1550 cm^{-1}) are observed [14,36]. With the increase in desorption temperature, the intensity of the characteristic peaks of Lewis acid sites decreases. The preservation of the pyridine peaks up to ca. 400 °C implies that the strength of Lewis acid sites on MoO_3/ZrO_2/MCM-41 catalyst is not very weak. These results further suggest that ZrO_2 as well dispersed particles probably forms a thin layer on the surface of MCM-41, and MoO_3 is coated on ZrO_2 and has little interaction with the silica wall.

3.2. Catalytic studies

The catalytic properties of MCM-41 supported MoO_3/ZrO_2 were investigated in the condensation of 2-methylfuran (MF) with acetone to synthesize 2,2-bis(5-methylfuryl) propane (BMP). Table 2 com-

Table 2
Condensation of 2-methylfuran with acetone over different catalysts[a]

Catalyst	Conversion of MF (%)	Selectivity to BMP (%)
Blank	0	–
Si-MCM-41	0	–
4% MoO_3/17% ZrO_2 + MCM-41[b,c]	26	95
4% MoO_3/13% ZrO_2/MCM-41[b]	77	96
4% MoO_3/13% ZrO_2/SiO_2[b]	44[d]	95
Al-MCM-41 (Si/Al = 31)	18	85
HY (Si/Al = 24)	52	94
HY (Si/Al = 2.7)	8[d]	93

[a] Reaction conditions: MF 1.8 g, acetone 3.2 g (molar ratio = 1:2.5), catalyst 0.18 g, reaction temperature 50 °C, reaction time 24 h.
[b] Catalyst calcined at 750 °C for 3 h.
[c] Mechanical mixture of 20% MoO_3/ZrO_2 and MCM-41.
[d] Aldol condensation of acetone was observed.

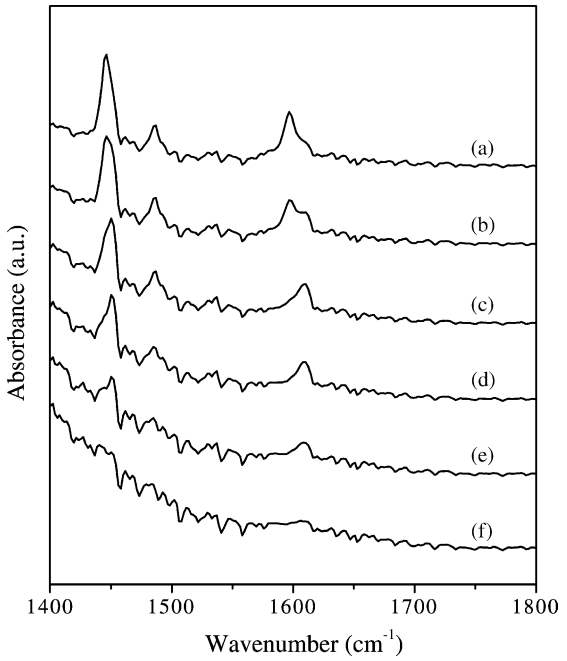

Fig. 7. In situ DRIFT spectra of pyridine adsorbed on 9% MoO_3/13% ZrO_2/MCM-41 calcined at 750 °C. Spectra recorded after evacuation at (a) 25 °C; (b) 100 °C; (c) 200 °C; (d) 300 °C; (e) 400 °C and (f) 500 °C.

pares the results of condensation of MF with acetone over MCM-41 mesoporous silica and MoO_3/ZrO_2 loaded on different supports. In the blank test reaction without any catalyst, no reaction occurs between MF and acetone. Pure siliceous MCM-41 also cannot catalyze the reaction. The three MoO_3/ZrO_2 containing catalysts give very high selectivities to BMP (90–96%). Among them, the catalysts prepared by impregnation gave higher MF conversion than the one prepared by physical mixing, and the one supported on MCM-41 was better than that on silica gel. These results are consistent with the acid amounts observed by NH_3-TPD studies. The sample, which contains the largest amount of acid sites, gives the highest activity. Because NH_3-TPD and DRIFT spectra show that these samples contain no strong acid sites, these results suggest that the condensation of 2-methylfuran with acetone does not need very strong acidity to catalyze the reaction. It is also noticeable that the MF conversion is very low over HY (Si/Al = 2.7) while the catalytic activity of HY (Si/Al = 24) is close to those of supported MoO_3/ZrO_2. Moreover, both the MF conversion and BMP selectivity are relatively low over Al-MCM-41 (Si/Al = 31). The extremely low catalytic activity of HY (Si/Al = 2.7) is attributed to the rapid deactivation of the catalyst, although no tar is detectable. The pores of HY were probably blocked by the oligomeric products of MF or the high ordered aldol condensation products of acetone since the dimer and trimer of aldol condensation products were detected in the liquid products over this catalyst. The product analysis also shows that the relatively low selectivity observed on Al-MCM-41 is due to some MF forming dimmer through alkylation.

We also compared the effect of the MF/acetone molar ratio on the MF conversion and BMP selectivity on 10% MoO_3/7% ZrO_2/MCM-41. When the stoichiometric ratio of MF/acetone (2:1) is used, the MF conversion is high (91%), but the BMP selectivity is relatively low (87%). When the amount of acetone is increased, the MF conversions decrease to 78–84%, while the BMP selectivity increases to 96%. These results are elucidated by assuming that acetone in this reaction is a reactant but can also serve as the solvent. Lack of solvent may accelerate the oligomerization of 2-methylfuran. As a result, the MF conversion is high but the BMP selectivity is low. Although addition of more acetone dilutes MF and results in lower conversion, it ultimately helps to suppress MF oligomerization. In the following studies, a relatively high acetone/MF ratio was used.

Table 3 shows the MF conversion and BMP selectivity over 10% MoO_3/7% ZrO_2/MCM-41 catalyst calcined at various temperatures. The MF conversion increases with the calcination temperature from 560

Table 3
Condensation of 2-methylfuran with acetone over 10% MoO_3/7% ZrO_2/MCM-41 catalyst calcined at different temperatures[a]

Calcined temperature (°C)	Conversion of MF (%)	Selectivity to BMP (%)
560	73	97
650	79	96
700	79	96
750	84	96
800	81	96

[a] Reaction conditions: MF 1.8 g, acetone 3.2 g (molar ratio = 1:2.5), catalyst 0.18 g, reaction temperature 50 °C, reaction time 24 h.

Table 4
Condensation of 2-methylfuran with acetone over MoO_3/ZrO_2/MCM-41 catalyst[a] with different MoO_3 loadings[b]

MoO_3 loading (%)	ZrO_2 loading (%)	Conversion of MF (%)	Selectivity to BMP (%)
0	14	19[c]	90
2	14	54	96
2	14	52[d]	96
4	13	77	96
9	13	83	96
14	13	80	95
17	13	61	97

[a] Catalyst calcined at 750 °C for 3 h.
[b] Reaction conditions: MF 1.8 g, acetone 3.2 g (molar ratio = 1:2.5), catalyst 0.18 g, reaction temperature 50 °C, reaction time 24 h.
[c] Aldol condensation of acetone was observed.
[d] After catalytic reaction for 24 h, the catalyst was filtered and calcined at 700 °C for 3 h, then used for the second time.

to 750 °C. However, the conversion decreases slightly when the calcination temperature reaches 800 °C. On the other hand, the BMP selectivity is independent of the calcination temperature and always has a value near 96%. It is also interesting to find that the optimal catalytic activity of MoO_3/ZrO_2/MCM-41 in the condensation of 2-methylfuran (MF) with acetone is very similar to that of sulfonic acid functionalized MCM-41, 81% versus 82% BMP yield. The latter was reported by Van Rhijn et al. [22] based on the same catalyst weight and reaction conditions.

Tables 4 and 5 compare the catalytic results of MoO_3/ZrO_2/MCM-41 with different MoO_3 or ZrO_2 contents. It is seen that ZrO_2/MCM-41 without MoO_3 shows very low catalytic activity, in both conversion and selectivity. The conversion of MF increases markedly with the increase in MoO_3 loading, while the selectivity of BMP is kept constant around 95%. The catalytic activity is consistent with the variation in surface area and the amount of acid sites. The 9% MoO_3/13% ZrO_2/MCM-41 has the largest amount of acid sites, and it shows the highest activity. On the 17% MoO_3/13% ZrO_2/MCM-41 sample, the activity decreases greatly. This sample shows very small amount of acid sites. In this case, the mesoporous structure of MCM-41 also collapses, and $ZrMo_2O_8$ is the predominant species. We also tested the activity of $ZrMo_2O_8$ sample, but it showed no catalytic activity. Over the catalysts with 8–10 wt.% MoO_3, nearly no change in the BMP selectivity is observed when the ZrO_2 content is changed. It is also noticeable that the 8 wt.% MoO_3/MCM-41 catalyst without ZrO_2 still has 46% MF conversion, indicating that MoO_3 is the main contribution to the acidity. However, the crystal structure of MCM-41 would be destroyed completely and a material of low surface area is obtained if MoO_3 is loaded along (as shown in Fig. 2(a)). By introducing $Zr(OH)_4$ on MCM-41 first before impregnation of MoO_3, the zirconium and molybdenum mixed oxide is formed and well dispersed on MCM-41 surfaces. Compared to the catalytic activity of MoO_3/MCM-41 catalyst without ZrO_2, the MF conversion increases markedly when ZrO_2 is also present and reaches a maximum value on the catalyst with 7–13 wt.% ZrO_2 contents. These results also indicate that a proper ratio of MoO_3/ZrO_2 is required in order to achieve the optimal catalytic activity. From the XRD studies, 9% MoO_3 and 13% ZrO_2 were the maximum loadings on MCM-41 to preserve the hexagonal structure without the formation of ZrO_2, MoO_3 crystals or $ZrMo_2O_8$ species. Consistently, MCM-41 with this loading of MoO_3/ZrO_2 gave the highest catalytic activity.

Table 5
Condensation of 2-methylfuran with acetone over MoO_3/ZrO_2/MCM-41 catalyst[a] with different ZrO_2 loadings[b]

MoO_3 loading (%)	ZrO_2 loading (%)	Conversion of MF (%)	Selectivity to BMP (%)
8	0	46	94
9	4	80	95
10	7	84	96
9	13	83	96
10	22	75	96

[a] Catalyst calcined at 750 °C for 3 h.
[b] Reaction conditions: MF 1.8 g, acetone 3.2 g (molar ratio = 1:2.5), catalyst 0.18 g, reaction temperature 50 °C, reaction time 24 h.

The deactivation behavior of the catalyst was examined by recycling the 2% MoO_3/14% ZrO_2/MCM-41 catalyst. The catalyst after 24 h reaction was filtered and calcined at 700 °C for 3 h, then used in the second time catalytic reaction. The result is shown in Table 4. The catalyst shows a minor decrease in the activity after the recycle, but the selectivity of BMP was found to still remain as high as 95–96%. These results indicate that the catalyst is not deactivated significantly and is of practical use.

4. Conclusions

MoO_3/ZrO_2 mixed oxides supported on siliceous MCM-41 were successfully prepared. The hexagonal ordered structure of MCM-41 was well preserved and no crystalline structure of MoO_3 or ZrO_2 appeared for up to 8–10 wt.% MoO_3 loading and 13–14 wt.% ZrO_2 loading. In these ranges of loading, the molybdena and zirconia are highly dispersed on the MCM-41 surface. XANES spectra showed that Mo was in octahedral coordination, and that no $ZrMo_2O_8$ crystals were formed. Impregnation of MCM-41 with MoO_3 tends to destroy the mesoporous structure; however, the structure was well preserved when the wall of MCM-41 was first coated with ZrO_2. A stronger interaction between MoO_3 and ZrO_2 than that of MoO_3 and SiO_2 was probably the reason. The MoO_3 and ZrO_2 loadings higher than 14 wt.% and 13%, respectively, would lead to the formation of $ZrMo_2O_8$ species. The MoO_3/ZrO_2/MCM-41 samples with well dispersed MoO_3 and ZrO_2 showed high surface areas and weak to medium acidity. Only Lewis acidity was observed on this material. The materials were highly efficient in catalyzing the condensation of 2-methylfuran and acetone with a high selectivity of 2,2-bis(5-methylfuryl)propane. MCM-41 with 9% MoO_3/13% ZrO_2 gave the highest catalytic activity. This combination was also the maximum amount of their loadings on MCM-41 with the hexagonal structure preserved and without the formation of ZrO_2, MoO_3 crystals or $ZrMo_2O_8$ species. Therefore, this loading should give the highest dispersion of Mo and Zr mixed oxide on MCM-41.

Acknowledgements

We gratefully acknowledge the financial supports from China Petroleum Corporation and the National Science Council of Taiwan.

References

[1] A. Corma, A. Martinez, Cat. Rev.-Sci. Eng. 35 (1993) 483.
[2] A. Corma, Chem. Rev. 95 (1995) 559.
[3] B.H. Davis, R.A. Keogh, R. Srinivasan, Catal. Today 20 (1994) 219.
[4] X. Song, A. Sayari, Cat. Rev.-Sci. Eng. 38 (1996) 329.
[5] M. Hino, K. Arata, J. Chem. Soc., Chem. Commun. (1988) 1259.
[6] M. Hino, K. Arata, Chem. Lett. (1989) 971.
[7] C.T. Kresge, M.E. Leonowicz, W.J. Roth, J.C. Vartuli, J.S. Beck, Nature 359 (1992) 710.
[8] A. Corma, A. Martinez, V. Martinez-Soria, J.B. Monton, J. Catal. 153 (1995) 25.
[9] A. Corma, A. Martinez, V. Martinez-Soria, J. Catal. 169 (1997) 480.
[10] T. Ookoshi, M. Onaka, Chem. Commun. (1998) 2399.
[11] S. Biz, M.L. Occeli, Cat. Rev.-Sci. Eng. 40 (1998) 329.
[12] C.-L. Chen, H.-P. Lin, S.-T. Wong, S. Cheng, C.-Y. Mou, in: Proceedings of the 3rd Seminar on Science and Technology-Catalysis, Fukuoka, Japan, 2000, p. 95.
[13] C.-L. Chen, S. Cheng, H.-P. Lin, S.-T. Wong, C.-Y. Mou, Appl. Catal. A 215 (2001) 21.
[14] Q.-H. Xia, K. Hidajat, S. Kawi, Chem. Commun. (2000) 2229.
[15] C.-L. Chen, T. Li, S. Cheng, H.-P. Lin, C.J. Bhongale, C.-Y. Mou, Microporous Mesoporous Mater. 50 (2001) 201.
[16] C.-L. Chen, T. Li, S. Cheng, H.-P. Lin, N.-P. Xu, C.-Y. Mou, Catal. Lett. 78 (2002) 223.
[17] J.E. Hall, USP 4 429 090 (1984);
A. Gandini, EPA 0 379 250 (1990).
[18] M. Choura, N.M. Belgacem, A. Gandini, Macromolecules 29 (1996) 3839.
[19] I.I. Patalakh, G.D. Gankin, R.A. Karakhanov, Izv. Vyssh. Uchebn. Zaved., Khim. Khim. Tekhnol. 35 (1992) 90.
[20] A. Gandini, M.N. Belgacem, Prog. Poly. Sci. 22 (1997) 1203.
[21] M.V. Sargent, F.M. Dean, in: A.R. Katrizky, C.W. Rees (Eds.), Furans and their benzo derivative: reactivity, in Comprehensive Heterocyclic Chemistry, vol. 4, Part 3, Pergamon Press, Oxford, 1997.
[22] W.M. Van Rhijn, D.E. De Vos, B.F. Sels, W.D. Bossaert, P.A. Jacobs, Chem. Commun. (1998) 317.
[23] D. Das, C.-M. Tsai, S. Cheng, Chem. Commun. (1999) 473.
[24] S.-T. Wong, H.-P. Lin, C.-Y. Mou, Appl. Catal. A 198 (2000) 103.
[25] D.-H. Cho, T.-S. Chang, S.-K. Ryu, Y.K. Lee, Catal. Lett. 64 (2000) 227.
[26] M. Auay, M. Quarton, P. Tarte, Powder Diffr. 2 (1987) 36.
[27] A. Khodakov, J. Yang, S. Su, E. Iglesia, A.T. Bell, J. Catal. 177 (1998) 343.
[28] K.-D. Chen, S.-B. Xie, E. Iglesia, A.T. Bell, J. Catal. 189 (2000) 421.
[29] S.-B. Xie, K.-D. Chen, A.T. Bell, E. Iglesia, J. Phys. Chem. B 104 (2000) 10059.
[30] H.-C. Hu, I.E. Wachs, S.R. Bare, J. Phys. Chem. 99 (1995) 10897.
[31] H. Aritani, T. Tanka, T. Funabiki, S. Yoshida, K. Eda, N. Sotani, M. Kudo, S. Hasegawa, J. Phys. Chem. 100 (1996) 19495.
[32] W. Chun, K. Asakura, Y. Iwasawa, J. Phys. Chem. B 102 (1998) 9006.
[33] S. Bare, G. Mitchell, J.J. Maj, G.E. Vrieland, J. Gland, J. Phys. Chem. 97 (1993) 6048.
[34] S.R. Bare, Langmuir 14 (1998) 1500.
[35] S.H. Elder, F.M. Cot, Y. Su, S.M. Heald, A.M. Tyryshkin, M.K. Bowman, Y. Gao, A.G. Joly, M.L. Balmer, A.C. Kolwaite, K.A. Magrini, D.M. Blake, J. Am. Chem. Soc. 122 (2000) 5138.
[36] B.-H. Li, R.D. Gonzalez, Catal. Today 46 (1998) 55.